ChemComm
Chemical Communications

Accepted Manuscript

This article can be cited before page numbers have been issued, to do this please use: P. Miao and Y. Tang, *Chem. Commun.*, 2020, DOI: 10.1039/D0CC01817A.

ROYAL SOCIETY OF CHEMISTRY

rsc.li/chemcomm

ChemComm

View Article Online
DOI: 10.1039/D0CC01817A

COMMUNICATION

Multipedal DNA walker for amplified detection of tumor exosomes†

Peng Miao,*[ab] and Yuguo Tang[a]

Received 00th January 20xx,
Accepted 00th January 20xx

DOI: 10.1039/x0xx00000x

We have fabricated an ultrasensitive exosome biosensor based on multipedal DNA walker with the core of target exosome. Specific recognition is achieved by introducing CD63 aptamer and facile separation is the benefit of magnetic Fe_3O_4@Au nanoparticles. Limit of detection down to 6 /μL is obtained with excellent selectivity.

Introduction

Exosomes are naturally produced nanoscale extracellular vesicles (30 to 150 nm) with the structure of a lipid bilayer membrane.[1-2] Exosomes carry considerable amounts of nucleic acids, proteins and lipids from originating cells and could transfer RNA or proteins to the cells they fuse with.[3] It is a critical pathway for the communication between parent cells and recipient cells.[4] Exosomes are secreted by many different cells including epithelial cells, leukocytes cells and tumor cells. As a result, they show great potential as biomarkers for the diagnosis of human diseases.[5-6] Monitoring of tumor exosomes has attracted great attention since the number of secreted exosomes becomes significantly increased during carcinogenesis compared with that in a healthy body.[7] The analysis of exosomes shows several merits over traditional biomarker assays. First, exosomes have been found in a variety of body fluids (e.g., blood, urine, semen, sputum and cerebrospinal fluids).[8] Most of these samples can be noninvasively collected and continuous monitoring is promised; second, exosome level is relatively abundant compared with other commonly applied biomarkers; third, exosomes have high stability with the lipid bilayer membrane structure and the samples can be preserved through several freeze-and-thaw cycles. Therefore, the development of exosomes detection methods is believed to hold great potential for tumor liquid biopsy.[9]

At present, ultracentrifugation (e.g., gradient ultracentrifugation) is the mainstream technique to gain exosomes, which purifies target vesicles from whole cells, cellular debris and subgroups based on their unique size and density. Recently, microfluidic devices have also been developed to isolate exosomes.[10] However, current analysis methods are subject to various defects or inconveniences. For example, the conventional Western blot, enzyme-linked immunosorbent assay and transmission electron microscopy (TEM) techniques require large sample volumes and extensive sample preparation processes;[11] flow cytometry shows limited sensitivity due to the weak light scattering from particles with diameters less than 100 nm;[12] nanoparticle tracking analysis (NTA) is a powerful technique but it is primarily designed for zeta-potential determination and specificity is insufficient.[13]

Electrochemistry is a powerful technique in various bioanalyses with the intrinsic merits of high sensitivity, simple setup, low cost, and versatile design.[14-17] In this work, we develop an ultrasensitive electrochemical method to determine tumor exosomes based on the construction of multipedal DNA walking nanomachine. DNA walker based strategy has attracted substantial attention for building up amplified sensing system.[18-19] A typical DNA walker could perform mechanical movement progressively across the designed track.[20-21] The walking rate could be enhanced by increasing the number of walker strands. Therefore, multipedal DNA walker is supposed to be beneficial to more efficient and sensitive analysis. In our previous work, we have constructed a multipedal DNA walker by the support of gold nanoparticles (AuNPs).[22] Herein, we immobilize multiple walker strands on a single target exosome, which is then exploited for autonomously walking based on the design of three-way junction structure.

Detailed working principle is illustrated in Scheme 1. First, magnetic nanoparticles are synthesized to aid the formation of multipedal DNA walker. Fe_3O_4@Au nanoparticles are prepared according to our previous work, which possess both merits of facile magnetic separation and rich modifiability by biomolecules.[23] DNA Probe A containing a short CD63 aptamer sequence are modified on the surface of Fe_3O_4@Au

[a] *CAS Key Lab of Bio-Medical Diagnostics, Suzhou Institute of Biomedical Engineering and Technology, Chinese Academy of Sciences, Suzhou 215163, P. R. China*
[b] *Department of Chemistry, New York University, New York 10003, United States*
Email: miaopeng@sibet.ac.cn; pm3084@nyu.edu

† Electronic Supplementary Information (ESI) available: details of experimental information, Figure S1-4 and Table S1-2.

nanoparticles. Due to the high recognition capability towards CD63 proteins on HeLa cell-derived exosomes,[24] the magnetic nanoparticles could be conjugated with exosomes. The designed walker strand of Probe B is then added, which also contains the aptamer sequence. Thus, a number of Probe B strands could be functionalized on the surface of exosomes and target exosome is used as the core of the multipedal walker. Magnetic separation is then carried out to remove unconjugated Probe B and the nanocomposites (Fe_3O_4@Au nanoparticles and exosome@Probe B) are then resuspended. After introducing Probe C and Nb.BbvCI nicking endonuclease (NEase), Probe A as the linker of exosome and Fe_3O_4@Au is cleaved. Meanwhile, Probe C is released and can be used to aid the cleavage of more Probe A coupled with NEase. As a result, after a second magnetic separation, exosome@Probe B (multipedal walker) is purified and kept in the supernatant. The electrode pre-modified with Probe D is incubated with the obtained multipedal walker solution in the presence of probe E. The strands (B, D, E) contain partially complementary sequences and many three-way junction structures are self-assembled between exosome and electrode interface. However, the duplex formed by Probe D and E contains the restriction site of Nb.BssSI NEase, thus, Probe D is cleaved, leading to the release of Probe B and E. Since the formed three-way junctions are not cleaved simultaneously, multipedal walker remains on the electrode. Some free Probe B strands on the surface of exosome participate the formation of new three-way junctions and multipedal walking is realized. Finally, a large amount of Probe D strands are cleaved and the 5' labeled methylene blue (MB) can no longer provide obvious electrochemical signal. By quantitative analysis of electrochemical response, target exosome level can be evaluated.

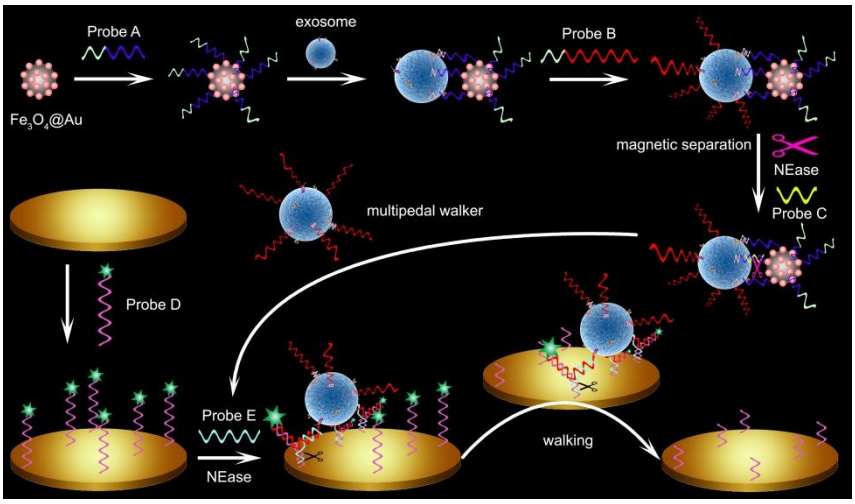

Scheme 1. Illustration of the multipedal DNA walking strategy for the detection of exosomes.

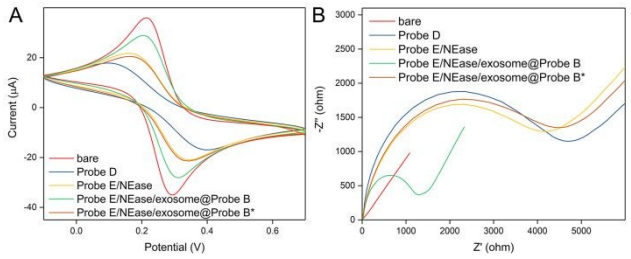

Figure 1. (A) Cyclic voltammograms and (B) nyquist diagrams of bare electrode, Probe D modified electrode, after incubation with probe E and NEase in the absence and presence of exosomes (with Probe B or Probe B*).

The morphology of collected exosomes is firstly characterized by TEM. Double-walled lipid membrane layers can be clearly observed and the mean diameter around 85 nm is determined by NTA, which are consistent with previous reports (Figure S1).[25] The successful synthesis of magnetic nanoparticles is confirmed by scanning electron microscope (SEM) image. The uniform spherical large particles around 150 nm are Fe_3O_4 cores and the small dots are AuNPs, which are well-distributed (Figure S2).

To verify the feasibility of this sensing strategy, we compare the electrochemical signals under different experimental stages. Cyclic voltammetry (CV) and electrochemical impedance spectroscopy (EIS) are performed to characterize the electrochemical properties with $[Fe(CN)_6]^{3-/4-}$ as redox label. As shown in Figure 1A, one pair of relatively sharp peaks are observed in the cyclic voltammogram of bare electrode. After modified with Probe D, due to the repellant of $[Fe(CN)_6]^{3-/4-}$ by the negatively charged DNA, the peaks are decreased significantly. In the presence of the fabricated multipedal walker, Probe D can be cleaved aided by Probe E and NEase. As a result, the repellant of $[Fe(CN)_6]^{3-/4-}$ is weakened with shorter DNA strands and the intensities of the peaks are recovered to certain extent. We have also performed control experiment with only Probe E/NEase. The peaks increase slightly, but are significantly lower than the case with multipedal walker. We have then replaced walker strand (Probe B) using a random sequence (Probe B*). The obtained peaks barely change compared with Probe E/NEase case, demonstrating the deficiency of DNA walking. Figure 1B shows corresponding nyquist plots of impedance. The impedance spectrum usually contains a semicircle portion at higher frequencies, which reflects the interfacial charge transfer resistance.[26] Bare electrode shows no semicircle domain, indicating excellent electron transfer rate of the substrate gold surface. With Probe D, a large semicircle appears, indicating the

increase of interfacial charge transfer resistance by the immobilized DNA. The multipedal DNA walking shortens Probe D, leading to the decrease of interfacial charge transfer resistance. The diameter of semicircle is thus dramatically decreased. However, the decreases of diameter are not obvious in the cases of two control experiments (Probe E/NEase and Probe E/NEase/exosome@Probe B).

Next, we have carried out square wave voltammetry (SWV) to characterize the electrochemical species of MB labeled at the 5' end of Probe D during different experimental stages. As shown in Figure 2, a significant current peak at around -0.3 V appears after the modification of Probe D on gold electrode interface. After exosome@Probe B mediated reactions, three-way junction structure forms, and Probe D is specially cleaved by NEase, which releases MB. With multipedal walking process, the electrochemical signal drops dramatically. However, if multipedal walker is not introduced or the recognition sequence inside is changed (Probe B*), exosomes cannot be captured for further walking reactions, which lead to nearly unchanged SWV peak intensities.

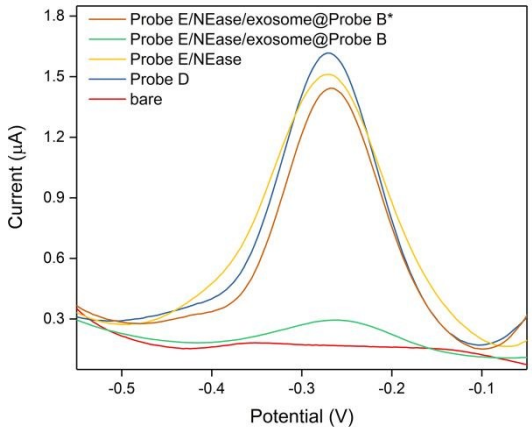

Figure 2. Square wave voltammograms of bare electrode, Probe D modified electrode, after incubation with probe E and NEase in the absence and presence of exosomes (with Probe B or Probe B*).

To achieve the best analytical performances, experimental parameters including concentrations of Probe D, Fe_3O_4@Au nanoparticles and reaction times of NEases are investigated. For Probe D, different concentrations of the DNA from 0.2 to 1.5 μM are modified on the surface of gold electrode and electrochemical responses of MB are measured. The peak current reaches the highest value with the concentration increased to 1 μM, which is used as the optimal Probe D concentration (Figure S3A). Similarly, different concentrations of Fe_3O_4@Au nanoparticles are applied for reactions. With the increase of concentration from 0.2 to 0.8 mg/mL, the SWV peak decreases and reaches the lowest value, demonstrating 0.8 mg/mL Fe_3O_4@Au nanoparticles are sufficient for the reactions (Figure S3B). The release of multipedal walker from magnetic nanoparticles and subsequent walking process rely on NEases. Therefore, the reaction times of Nb.BbvCI and Nb.BssSI are key factors. We have separately checked the effects of reaction times on the SWV peak currents. After comparison, optimal reaction times of 60 min and 90 min are selected for following experiments, respectively (Figure S3C and S3D). In addition, we have recorded the values of charge transfer resistance (R_{ct}) over Nb.BssSI reaction time. At the beginning, it gradually decreases, indicating the release of part of probe D strands. A sudden drop appears at the critical time of 90 min, which is due to the fact that after cleaving nearly all Probe D strands on the electrode surface, exosome@Probe B is also released and charge transfer resistance becomes much smaller (Figure S3D).

Under these optimized conditions, standard exosomes with a series of concentrations are introduced in the sensing system to study the detection range and sensitivity. SWV curves are recorded and shown in Figure 3A. With the increase of exosomes concentration, SWV peak current decreases, indicating the formation of more multipedal walkers. Detailed relationship between exosome concentration and electrochemical response is depicted in Figure 3B. A linear equation is established between the variation of SWV peak current and logarithm of exosome concentration as follows:

$$y = 0.454\,x - 0.330\ (n = 3;\ R^2 = 0.998)$$

in which y is the decreased SWV peak while x is the logarithmic concentration of exosome. The linear range is from 10 to 2000 /μL and the limit of detection (LOD) is 6 /μL, which is lower than most current reported methods (Table S1). This method also shows excellent reproducibility. We have employed three sets of Fe_3O_4@Au nanoparticles and three independent electrodes for the detection of different amounts of exosomes. The obtained results are consistent correspondingly and the relative standard deviations (RSD) are less than 5%, which are acceptable for an analytical tool (Figure S4).

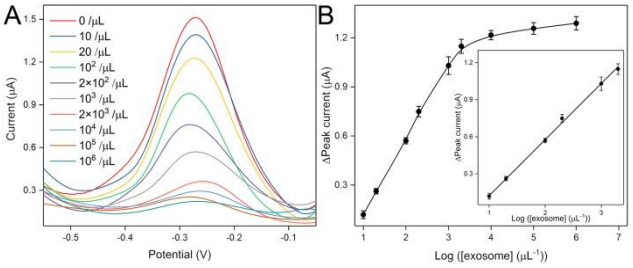

Figure 3. (A) Square wave voltammograms for the detection of exosomes with the concentrations of 0, 10, 20, 10^2, 2×10^2, 10^3, 2×10^3, 10^4, 10^5, 10^6 /μL. (B) Calibration plot of the SWV peak current variation versus the logarithmic concentration of exosomes. Inset shows the linear range.

To check the discrimination capability of this strategy, we have introduced another cell line MCF-10A and collect the secreted non-tumorigenic exosomes for comparison. The selectivity of this method relies on the specific aptamer that targets CD63 on the outer phospholipid bilayer of exosomes. In the presence of the same concentrations of exosomes, HeLa cells create much larger electrochemical signal variations compared with MCF-10A cells, which is because MCF-10A cells express lower levels of CD63 (Figure 4).[27] Therefore, good selectivity of tumor exosomes is demonstrated.

To further ensure the anti-jamming capability of this sensing system in complex biological environment, we have determined exosome concentrations in serum samples, which contain abundant highly concentrated components. As listed in Table 1, the calculated concentrations of exosomes are almost the same as actually spiked values. The results indicate that this method may have potential clinical applications with excellent practical utility.

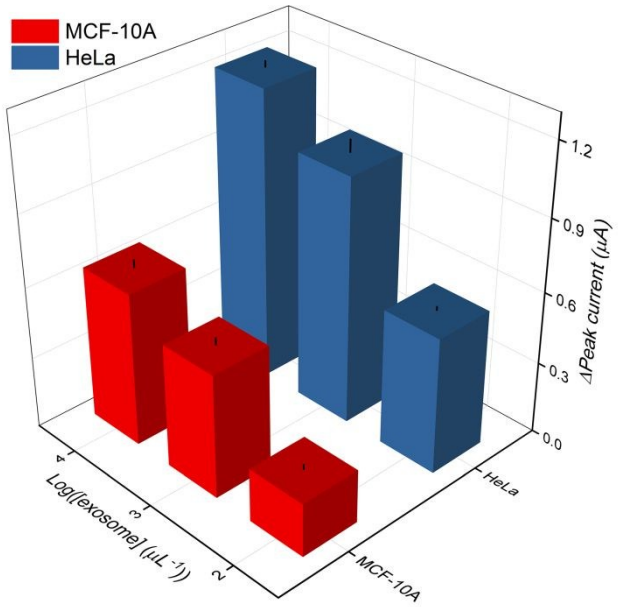

Figure 4. Selectivity investigation toward exosomes secreted from different parent cells.

Table 1. Detection of exosomes in 10% serum samples.

Sample	Spiked (/μL)	Detected (/μL)	Recovery (%)	RSD (%)
Serum 1	200	210	105.0	3.8
	2000	2130	106.5	4.7
Serum 2	200	215	107.5	2.9
	2000	1940	97.0	4.6

Conclusions

In summary, we have fabricated a highly sensitive and selective approach to detect tumor cell-derived exosomes, which presents three merits as a powerful analytical tool. First, magnetic nanomaterials facilitate operation and working efficiency. Second, the ingenious design using target exosome as the core of multipedal DNA walker simplifies the sensing system; meanwhile, the signal amplification efficiency is significantly improved. Third, three-way junction structure constructed on the surface of electrode is the basic walking unit, which can be easily realized and controlled. We believe this multipedal DNA walker based exosome biosensor may shed new light on DNA nanomachine and cancer diagnostics.

Acknowledgements

This work is supported by the National Natural Science Foundation of China (81771929) and China Scholarship Council (201904910056).

Conflicts of interest

There are no conflicts to declare.

Notes and references

View Article Online
DOI: 10.1039/D0CC01817A

1. R. Kalluri and V. S. LeBleu, Science, 2020, **367**, eaau6977.
2. M. X. Wu, Y. S. Ouyang, Z. Y. Wang, R. Zhang, P. H. Huang, C. Y. Chen, H. Li, P. Li, D. Quinn, M. Dao, S. Suresh, Y. Sadovsky and T. J. Huang, *Proc. Natl. Acad. Sci. U. S. A.*, 2017, **114**, 10584-10589.
3. H. Valadi, K. Ekstrom, A. Bossios, M. Sjostrand, J. J. Lee and J. O. Lotvall, *Nat. Cell Biol.*, 2007, **9**, 654–659.
4. M. Tkach and C. Thery, *Cell*, 2016, **164**, 1226-1232.
5. E. Delorme-Axford, R. B. Donker, J. F. Mouillet, T. J. Chu, A. Bayer, Y. S. Ouyang, T. Y. Wang, D. B. Stolz, S. N. Sarkar, A. E. Morelli, Y. Sadovsky and C. B. Coyne, *Proc. Natl. Acad. Sci. U. S. A.*, 2013, **110**, 12048-12053.
6. J. Linxweiler and K. Junker, *Nat. Rev. Urol.*, 2020, **17**, 62-62.
7. J. Skog, T. Wurdinger, S. van Rijn, D. H. Meijer, L. Gainche, M. Sena-Esteves, W. T. Curry, B. S. Carter, A. M. Krichevsky and X. O. Breakefield, *Nat. Cell Biol.*, 2008, **10**, 1470–1476.
8. S. Wan, L. Q. Zhang, S. Wang, Y. Liu, C. C. Wu, C. Cui, H. Sun, M. L. Shi, Y. Jiang, L. Li, L. P. Qiu and W. H. Tan, *J. Am. Chem. Soc.*, 2017, **139**, 5289-5292.
9. L. Wang, Y. C. Yang, Y. F. Liu, L. M. Ning, Y. Xiang and G. X. Li, *Chem. Commun.*, 2019, **55**, 2708-2711.
10. T. L. Zhang, Z. Y. Hong, S. Y. Tang, W. H. Li, D. W. Inglis, Y. Hosokawa, Y. Yalikun and M. Li, *Lab Chip*, 2020, **20**, 35-53.
11. X. Q. Wang, F. A. Shah, F. Vazirisani, A. Johansson, A. Palmquist, O. Omar, K. Ekstrom and P. Thomsen, *Biomaterials*, 2020, **230**, 119571.
12. A. Yokoi, A. Villar-Prados, P. A. Oliphint, J. H. Zhang, X. Z. Song, P. De Hoff, R. Morey, J. S. Liu, J. Roszik, K. Clise-Dwyer, J. K. Burks, T. J. O'Halloran, L. C. Laurent and A. K. Sood, *Sci. Adv.*, 2019, **5**, eaax8849.
13. Y. T. Yang, G. X. Shen, H. Wang, H. X. Li, T. Zhang, N. J. Tao, X. T. Ding and H. Yu, *Proc. Natl. Acad. Sci. U. S. A.*, 2018, **115**, 10275-10280.
14. J. Zhang, H. Chen, Y. Cao, C. Feng, X. L. Zhu and G. X. Li, *Anal. Chem.*, 2019, **91**, 1005-1010.
15. J. F. Chang, X. Wang, J. Wang, H. Y. Li and F. Li, *Anal. Chem.*, 2019, **91**, 3604-3610.
16. Y. Liu, T. T. Li, C. X. Ling, Z. Chen, Y. Deng and N. Y. He, *Chin. Chem. Lett.*, 2019, **30**, 2211-2215.
17. L. Ge, Q. Hong, H. Li, C. C. Liu and F. Li, *Adv. Funct. Mater.*, 2019, **29**, 1904000.
18. J. Huang, L. Y. Zhu, H. X. Ju and J. P. Lei, *Anal. Chem.*, 2019, **91**, 6981-6985.
19. H. Chai and P. Miao, *Anal. Chem.*, 2019, **91**, 4953-4957.
20. Z. Q. Chen, C. Wang, L. J. Hao, R. Gao, F. Li and S. F. Liu, *Biosens. Bioelectron.*, 2019, **128**, 104-112.
21. Y. L. Wang, L. Y. Xia, C. Y. Wei, H. H. Wang, H. J. Wang, R. Yuan and S. P. Wei, *Chem. Commun.*, 2019, **55**, 13082-13084.
22. P. Miao and Y. G. Tang, *Anal. Chem.*, 2019, **91**, 15187-15192.
23. P. Miao, Y. G. Tang and L. Wang, *ACS Appl. Mater. Interfaces*, 2017, **9**, 3940-3947.
24. Q. X. Zhang, F. Wang, H. X. Zhang, Y. Y. Zhang, M. L. Liu and Y. Liu, *Anal. Chem.*, 2018, **90**, 12737-12744.
25. J. Chen, H. M. Meng, Y. An, X. Geng, K. R. Zhao, L. B. Qu and Z. H. Li, *Talanta*, 2020, **209**, 120510.
26. X. L. Zhu, Y. Y. Chen, C. Feng, W. Wang, B. Bo, R. X. Ren and G. X. Li, *Anal. Chem.*, 2017, **89**, 4131-4138.
27. Y. Cao, L. L. Li, B. Han, Y. Wang, Y. H. Dai and J. Zhao, *Biosens. Bioelectron.*, 2019, **141**, 111397.

View Article Online
DOI: 10.1039/D0CC01817A

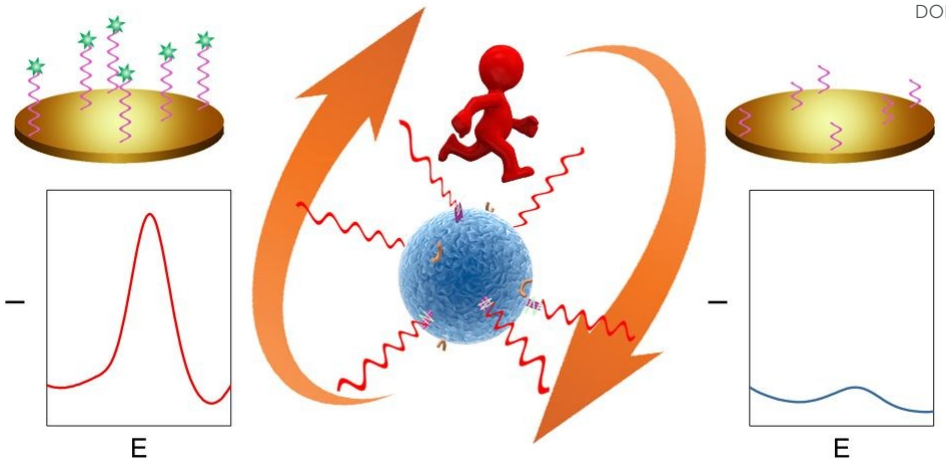

A novel electrochemical biosensor for exosomes is proposed based on multipedal DNA walking strategy. The limit of detection down to 6 /μL is obtained with excellent selectivity.